Nuclear Engineering and Technology 55 (2023) 2797–2801

Contents lists available at ScienceDirect

Nuclear Engineering and Technology

journal homepage: www.elsevier.com/locate/net

Original Article

Feasibility study of CdZnTe and CdZnTeSe based high energy X-ray detector using linear accelerator

Beomjun Park [a, b, c], Juyoung Ko [a], Jangwon Byun [a], Byungdo Park [d], Man-Jong Lee [a, b, **], Jeongho Kim [d, *]

[a] Department of Chemistry, Konkuk University, Seoul, 143-701, Republic of Korea
[b] Advanced Crystal Material/Device Research Center, Konkuk University, Seoul, 143-701, Republic of Korea
[c] Interdisciplinary Program in Precision Public Health, Korea University, Seoul, 02841, Republic of Korea
[d] Department of Radiation Oncology, Samsung Changwon Hospital, Sungkyunkwan University School of Medicine, Changwon, 51353, Republic of Korea

ARTICLE INFO

Article history:
Received 27 March 2023
Received in revised form
25 April 2023
Accepted 1 May 2023
Available online 5 May 2023

Keywords:
CdZnTe
CdZnTeSe
Radiation dosimeter
Coefficient of determination
Relative standard deviation

ABSTRACT

CdZnTeSe (CZTS) has attracted attention for applications in X- and gamma-ray detectors owing to its improved properties compared to those of CdZnTe (CZT). In this study, we grew and processed single crystals of CZT and CZTS using the Bridgeman method to confirm the feasibility of using a dosimeter for high-energy X-rays in radiotherapy. We evaluated their linearity and precision using the coefficient of determination (R^2) and relative standard deviation (RSD). CZTS showed sufficient RSD values lower than 1.5% of the standard for X-ray dosimetry, whereas CZT's RSD values increased dramatically under some conditions. CZTS exhibited an R^2 value of 0.9968 at 500 V/cm, whereas CZT has an R^2 value of 0.9373 under the same conditions. The X-ray response of CZTS maintains its pulse shape at various dose rates, and its properties are improved by adding selenium to the CdTe matrix to lower the defect density and sub-grain boundaries. Thus, we validated that CZTS shows a better response than CZT to high-energy X-rays used for radiotherapy. Further, the applicability of an onboard imager, a high-energy X-ray (>6 MV) image, is presented. The proposed methodology and results can guide future advances in X-ray dose detection.
© 2023 Korean Nuclear Society, Published by Elsevier Korea LLC. This is an open access article under the CC BY-NC-ND license (http://creativecommons.org/licenses/by-nc-nd/4.0/).

1. Introduction

The objective of radiotherapy is to kill tumors and minimize side effects [1]. To achieve these goals, treatment precision needs to be enhanced the through equipment quality assurance (QA), patient-specific QA, and in vivo dosimetry. Various radiation detectors have been used for QA and in vivo dosimetry during radiation therapy. Metal oxide semiconductor field-effect transistor (MOSFET) dosimeters have been widely used as in vivo dosimeters because of their small size, room-temperature operation, and real-time measurement capabilities. However, MOSFET has the disadvantage of a finite lifetime [2].

For decades, CdTe-based semiconductors have been the leading materials for X- and gamma-ray detectors operating at room temperature [3,4]. Particularly, CdZnTe (CZT) is the most promising material and is widely used in various fields such as high-energy physics, aerospace, and diagnosis [4–7]. Moreover, CdTe-based semiconductors can be used as dosimeters [8]. CdTe-based semiconductors exhibit high effective atomic numbers and detection efficiencies. Additionally, CdTe-based detectors exhibit high charge-collection efficiency, low leakage current, and sufficient electron carrier transport characteristics [4]. Thus, they are suitable dose detectors for radiotherapy. Besides, there are no reported finite-lifetime characteristics of CdTe-based semiconductors, which is a limitation of MOSFET dosimeters.

Recently, bandgap engineering, including optimized zinc (Zn) content and selenium (Se) doping, has been attempted to improve the performance of CZTs [8–12]. Increasing the Zn content in the CZT composition almost linearly increases the band gap, reducing the shot noise and leakage current [9,13]. Moreover, the addition of Se to the CdZnTe matrix reduces the density of subgrain boundaries, Zn segregation, and other defect densities [[9–12,14,15]].

* Corresponding author.
** Corresponding author. Department of Chemistry, Konkuk University, Seoul, 143-701, Republic of Korea.
E-mail addresses: leemtx@konkuk.ac.kr (M.-J. Lee), jeongho5248@gmail.com (J. Kim).

https://doi.org/10.1016/j.net.2023.05.003
1738-5733/© 2023 Korean Nuclear Society, Published by Elsevier Korea LLC. This is an open access article under the CC BY-NC-ND license (http://creativecommons.org/licenses/by-nc-nd/4.0/).

CdZnTeSe (CZTS) exhibits better spectroscopic properties than CZT [16,17].

In this study, $Cd_{0.9}Zn_{0.1}Te$ (CZT) and $Cd_{0.9}Zn_{0.1}Te_{0.98}Se_{0.02}$ (CZTS) ingots were grown by the Bridgman technique and exposed to high energy X-rays generated by a linear accelerator (Linac) after synthesizing the X-ray detector by standard fabricating procedures. We have evaluated the feasibility of CZTS in terms of linearity and precision in the field of radiotherapy for the first time. Furthermore, we proposed the possibility of applying CZTS to an onboard imager, which is the image sensor of a linear accelerator.

2. Materials and methods

2.1. Crystal growth and detector fabrication

Both the CZT and CZTS ingots were grown using the Bridgman method with a stoichiometric composition of $Cd_{0.9}Zn_{0.1}Te_1$ and $Cd_{0.9}Zn_{0.1}Te_{0.98}Se_{0.02}$, and then sliced into flat wafers. These planar wafers were polished with sandpaper/polishing cloth using alumina abrasive, chemically etched with 2% bromine in MeOH, electrode deposited, and passivated. Details of the growth and fabrication are similar to those in previous studies [11,18], except for the stoichiometry. Electrode deposition was performed using an electroless method based on $AuCl_3$ solution. Passivation was achieved by immersing the CZT and CZTS samples in a hydroperoxide solution for 180 s [19]. The physical dimensions of the processed detectors were 5.0 × 5.0 × 2.5 for CZTS and 6.1 × 5.6 × 3.1 for CZT.

The detectors were placed in contact with a custom-made PCB board with a gold wire and conductive epoxy (Circuitworks conductive epoxy, Chemtronics) to separate the anode and cathode signals, as shown in Fig. 1(a). Conductive epoxy was used instead of tin soldering to minimize thermal damage. The PCB was then soldered to the wires and connected to the data acquisition system, as shown in Fig. 1(b).

2.2. Experimental conditions for obtaining high energy X-ray responses

The fabricated detectors were installed inside the Linac (TrueBeam, Varian) of Samsung Changwon Hospital, where the X-ray energy, source-to-detector distance, and field size were set to 6 MV, 100 cm, and 10 × 10 cm^2, respectively. The dose on the detector was designed to be a nominal 1 Gy by setting 100 monitoring unit (MU) and the appropriate thickness of soft tissue-equivalent materials, such as a water-solid phantom and bolus (Fig. 1). X-ray responses were obtained using a Keithley 2636 B at different dose rates ranging from 100 to 600 MU/min. Identical experiments were performed under various electric fields (100, 300, and 500 V/cm).

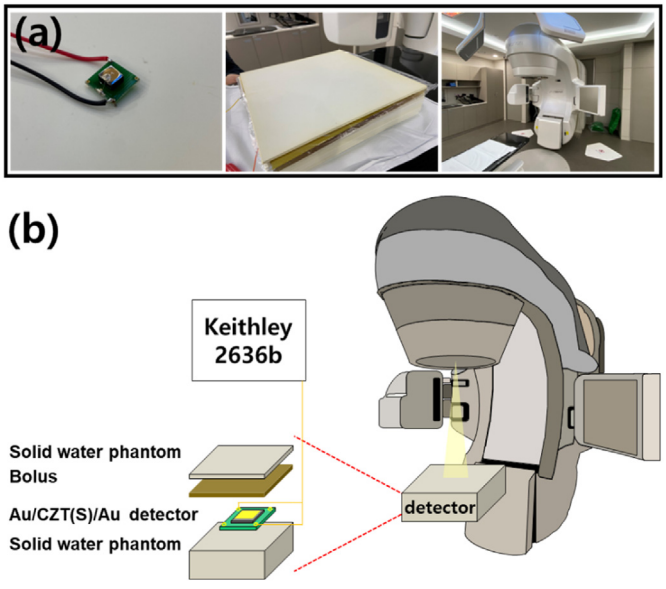

Fig. 1. (a) Photographs and (b) schematics of the sample and detector used for X-ray evaluation.

2.3. Data correction and X-ray evaluation

Simulations were performed using MATLAB R2022b to compensate for the differences in the thicknesses of the detectors. The relative absorption with different CZTS thicknesses was calculated from the incident Linac input spectrum [20]. The mass attenuation coefficient at each energy was calculated from the data of NIST [21], and the density of CZTS was set to 5.8 g/cc, the same as that of CZT [22,23]. Each calculated count was multiplied by the energy of the corresponding X-ray photon and then summarized into one value, called the dose factor at X mm (D_X). Moreover, because the dose factor included only the effect of the thickness, the active area of the photocurrent obtained by the CZTS detector was corrected. The final correction factor was multiplied by the photocurrent obtained using the CZTS detector.

$$Correction\ factor = \frac{D_{3.1}}{D_{2.5}} \times \frac{active\ area\ of\ CZT}{active\ area\ of\ CZTS} \quad (1)$$

Coefficient of determination (R^2) and relative standard deviation (RSD) were used to evaluate the linearity and precision of the X-ray detectors, respectively. The former was calculated by fitting a correlation between the dose rate and photocurrent intensity, and the latter was calculated using the following equation [24]:

$$RSD(\%) = \left[\frac{\left\{\sum (X_i - X_{ave})^2 / n\right\}^{0.5}}{X_{ave}}\right] \times 100 \quad (2)$$

3. Results and discussion

Corrections must be performed to compensate for the different physical dimensions of each detector. Different areas can be corrected by multiplying them with the active area of the detector. However, the absorption of X-ray photons of different thicknesses is complicated because of the multi-exponential attenuation of X-rays in materials [21]. Therefore, the X-ray spectrum used in this study was obtained, and the relative absorption rate according to the thickness of CZTS at each energy level was simulated, as shown in Fig. 2. For the photocurrent correction corresponding to the detector dose, the energy of the X-ray spectrum was multiplied by each corresponding count and summarized into a single value. The calculated correction factor was 1.676, as shown in Eq. (1) (correction factor = 1.226482 × $\frac{6.1\times5.6}{5.0\times5.0}$). This value was adopted for all the photocurrent values obtained using the CZTS detector.

In a semiconductor detector, the path length of a charge carriers is determined by the product of mobility, lifetime, and electric field ($\mu\tau E$). Therefore, the electric field of each detector was set to 100, 300, and 500 V/cm, as shown in Fig. 3–5, respectively. For appropriate evaluation of a semiconductor detector, same electric field should be applied. Fig. 3 shows the photocurrent and RSD values at various dose rates at 100 V/cm. For both detectors, the tendency of the photocurrent showed a linear correlation with the dose rate, with R^2 values of 0.9997 for CZTS and 0.9963 for CZT. These values,

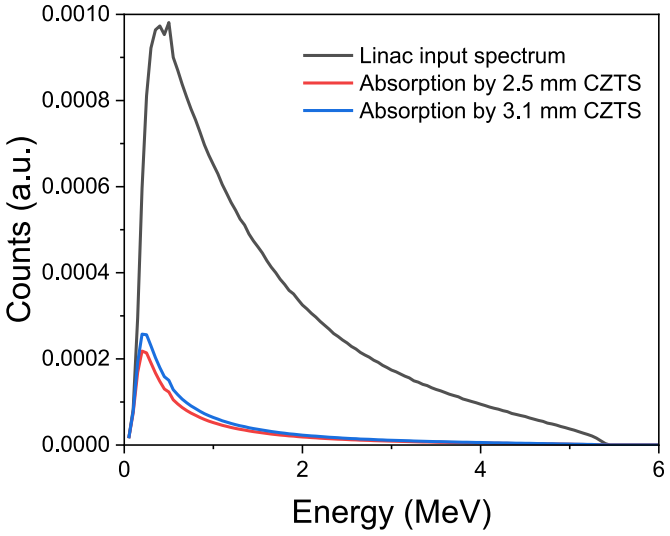

Fig. 2. Incident input spectrum of Linac [20] and simulated spectra of different thicknesses of the CZTS detectors calculated for the correction of obtained photocurrent.

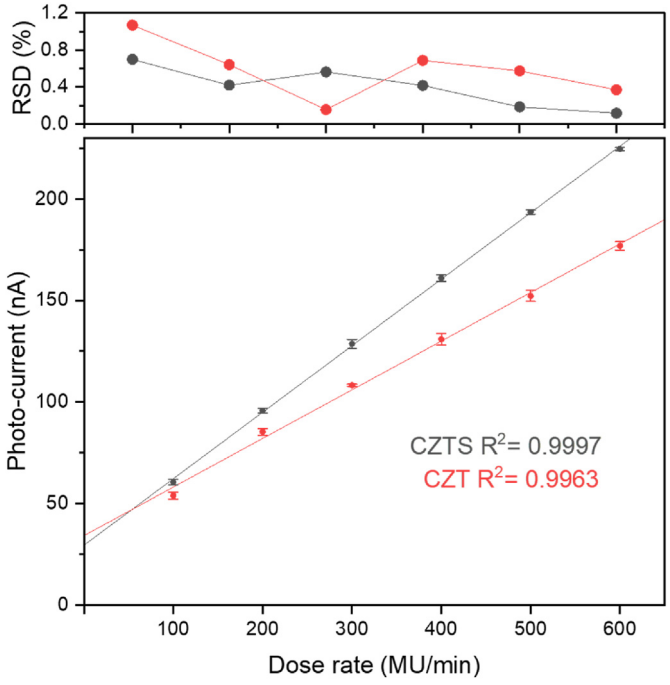

Fig. 3. Photocurrent and RSD values of CZT (red) and CZTS (gray) for different dose rates at 100 V/cm. (For interpretation of the references to colour in this figure legend, the reader is referred to the Web version of this article.)

which are close to 1, demonstrate the good linearity between the dose rate and the photocurrent of the CZT and CZTS detectors biased at 100 V/cm. Because the R^2 values were calculated from the mean value of the photocurrent at each dose rate, the RSD value was considered as a precision check. The RSD values were within 1%, except for the photocurrent of 100 MU/min in the CZT detector. However, 1.2% of the RSD was distinct, even within the standard value (1.5%) for evaluating the reproducibility of radiation dose detector [24–26].

Fig. 4 shows the photocurrent and RSD values at 300 V/cm under the same conditions. A higher bias voltage improves the path

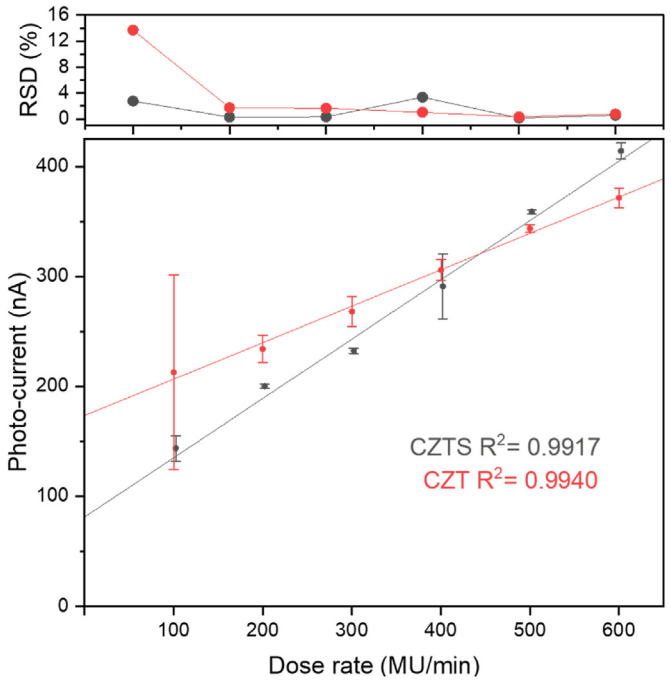

Fig. 4. Photocurrent and RSD values of CZT (red) and CZTS (gray) for different dose rates at 300 V/cm. (For interpretation of the references to colour in this figure legend, the reader is referred to the Web version of this article.)

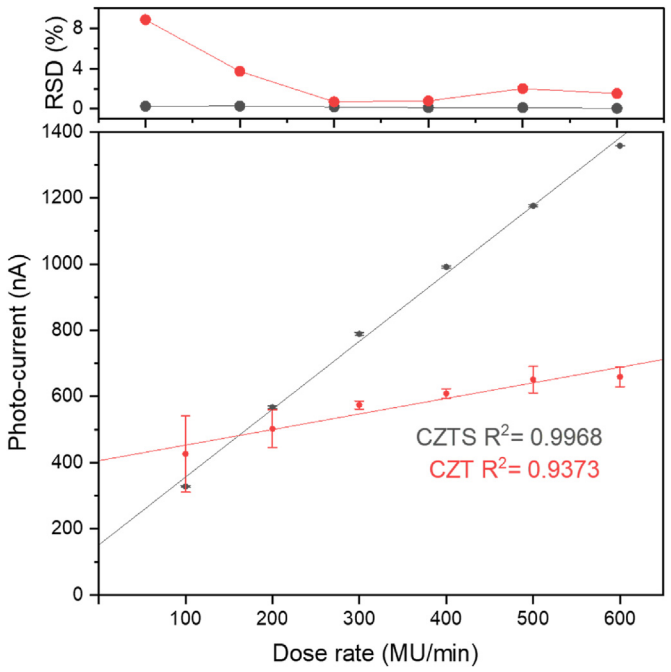

Fig. 5. Photocurrent and RSD values of CZT (red) and CZTS (gray) for different dose rates at 500 V/cm. (For interpretation of the references to colour in this figure legend, the reader is referred to the Web version of this article.)

length by increasing the electric field, which improves the charge collection efficiency (CCE) [27]. Therefore, photocurrent increased at all dose rates in Fig. 4 compared to those at a lower electric field (100 V/cm), as shown in Fig. 3. The linearity of each detector was less obvious than that for 100 V/cm, with linearity of 0.9917 for CZTS and 0.9940 for CZT. Moreover, the RSD value of CZT was larger than that shown in Fig. 3, which indicates that the photocurrent

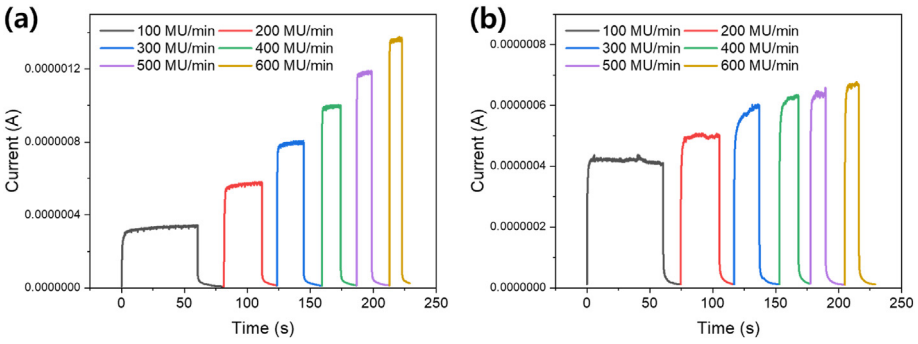

Fig. 6. Pulse shapes at 500 V/m with various dose rates obtained from (a) CZTS (b) and CZT.

fluctuated in all X-ray shots. When the dose rate was set to 100 MU/min, RSD value reached 14%, indicating low reproducibility. Collectively, the characteristics of CZTS were superior to those of CZT at 300 V/cm despite the lower R^2 values. As mentioned previously, R^2 value was calculated as the mean value of the photocurrent. To observe a detailed effect of voltage variation, we applied an electric field of 500 V/cm, which is close to the degree of spectroscopic characterization.

As shown in Fig. 5, the photocurrent at each dose rate increases with bias voltage. The linearity and precision of CZT deteriorated significantly at higher voltages. This stems from the relatively unstable nature of CZT at high voltages. An R^2 value of 0.9373 was obtained, and RSD values of greater than 1.5% were obtained at 100, 200, 500, and 600 MU/min. In contrast, CZTS exhibited more stable and prominent characteristics. The photocurrent maintained linearity with the dose rate, with an R^2 value of 0.9968. RSD values were also within 1.5% for all exposures at different dose rates.

Fig. 6 shows the pulse shapes of CZTS and CZT depending on the dose rate at 500 V/cm. In both detectors, photocurrent increased with the dose rate. Simultaneously, the exposure time was shortened because the total dose was fixed at 100 MU while the dose rate varied from 100 to 600 MU/min. However, the incremental intervals of the photocurrents in CZT and CZTS were different, as shown in Fig. 5. The CZTS photocurrent exhibited small changes at different dose rates; however, CZT exhibited different pulse shapes at all dose rates. The pulse shape affects dose detection. Therefore, an unreproducible pulse shape can serve as an unstable characteristic of CZT detectors (Fig. 5). The stability of an X-ray response depends on various parameters such as defects, bias voltage, and incident X-rays. In this case, all conditions were identical, except for the stoichiometry of the detectors (CZT and CZTS). Therefore, better response characteristics to X-rays resulted from improved CZTS properties, including low defect density, reduced subgrain boundaries, and networks [14–17]. Interestingly, the corrected photocurrent of CZTS was higher than that of CZT despite the lower atomic number of Se compared to that of Te. In other words, the addition of 2% Se does not show a significant decrease in the collected photocurrent; but rather, the reduced defects by selenium addition played a greater role in improving X-ray response and increasing the charge collected by the crystal. Therefore, CZTS is more suitable as an X-ray dose detector than CZT in terms of linearity and precision. Moreover, it can be used as an onboard imager (OBI) for high-energy X-rays when pixelated CZTS detectors are introduced. Furthermore, the methodology used in this study can provide guidance for other radiation-dose detectors.

4. Conclusion

In this study, the validity of CZT and CZTS as X-ray dose detectors in radiotherapy was confirmed for the first time in terms of linearity and precision. Both semiconductors were prepared using the same process: Bridgman growth, lapping, polishing, chemical etching, deposition, and passivation. Linearity and precision were determined using the coefficient of determination (R^2) and relative standard deviation (*RSD*), respectively. Correction factors were calculated to calibrate the sample dimensions of two different samples (CZT and CZTS). The precision of CZTS detector displayed prominent *RSD* values of less than 1.5% in all applied electric fields, whereas the *RSD* values of CZT fluctuated under some conditions. The linearity of CZTS at 500 V/cm was sufficient, as confirmed by the R^2 value of 0.9968. The pulse shape maintained a similar trend at dose rates ranging from 100 to 600 MU/min, which may be a result of the addition of Se to the CdTe matrix to improve properties such as low defect density and reduced subgrain boundaries and their networks. Thus, CZTS showed a better response than CZT to high-energy X-rays used for radiotherapy.

Declaration of competing interest

The authors declare that they have no known competing financial interests or personal relationships that could have appeared to influence the work reported in this paper.

Acknowledgements

This research was supported by the Challengeable Future Defense Technology Research and Development Program through the Agency for Defense Development (ADD) funded by the Defense Acquisition Program Administration (DAPA) in 2022 (No. UI220006TD).

References

[1] J.H. Kim, B. Kim, W.-G. Shin, J. Son, C.H. Choi, J.M. Park, Ui-J. Hwang, J. in Kim, S. Jung I, 3D star shot analysis using MAGAT gel dosimeter for integrated imaging and radiation isocenter verification of MR-Linac system, J. Appl. Clin. Med. Phys. 23 (2022), e13615.
[2] M. Ciocca, V. Piazzi, R. Lazzari, A. Vavassori, A. Luini, P. Veronesi, V. Galimberti, M. Intra, A. Guido, G. Tosi, U. Veronesi, R. Orecchia, Real-time in vivo dosimetry using micro-MOSFET detectors during intraoperative electron beam radiation therapy in early-stage breast cancer, Radiother. Oncol. 78 (2006) 213–216.
[3] T.E. Schlesinger, Semiconductors and semimetals semiconductors for room temperature nuclear detector applications, Semicond, Semimetals 43 (1995) 240.
[4] S.D. Sordo, L. Abbene, E. Caroli, A.M. Mancini, A. Zappettini, P. Ubertini, Progress in the development of CdTe and CdZnTe semiconductor radiation detectors for astrophysical and medical applications, Sensors 9 (5) (2009) 3491–3526.
[5] S. Watanabe, et al., The Si/CdTe semiconductor Compton camera of the ASTRO-H soft gamma-ray detector (SGD), Nucl. Instrum. Methods. Phys. Res. B NUCL INSTRUM METH A 765 (2014) 192–201.
[6] K. Iniewski, CZT detector technology for medical imaging, J. Instrum. 9 (2014)

11. C11001.
[7] F. Glasser, V. Gerbe, P. Ouvrier-Buffet, M. Accensi, J.L. Girard, M. Renaud, J.L. Gersten-Mayer, CdZnTe high-energy radiography detector, Nucl. Instrum. Methods. Phys. Res. B NUCL INSTRUM METH A 458 (2001) 544–550, 1-2.
[8] J. Byun, Y. Kim, J. Seo, E. Kim, K. Kim, A. Jo, W. Lee, B. Park, Development and evaluation of photon-counting $Cd_{0.875}Zn_{0.125}Te_{0.98}Se_{0.02}$ detector for measuring bone mineral density, Phys. Eng. Sci. Med. (2023) 1–9.
[9] B. Park, Y. Kim, J. Seo, J. Byun, V. Dedic, J. Franc, A.E. Bolotnikov, R.B. James, K. Kim, Bandgap engineering of $Cd_{1-x}Zn_xTe_{1-y}Se_y$ ($0< x< 0.27$, $0< y< 0.026$, Nucl. Instrum. Methods. Phys. Res. B NUCL INSTRUM METH A 1036 (2022), 166836.
[10] U.N. Roy, G.S. Camarda, Y. Cui, R.B. James, Advances in CdZnTeSe for radiation detector applications, Radiation 1.2 (2021) 123–130.
[11] S. Hwang, H. Yu, A.E. Bolotnikov, R.B. James, K. Kim, Anomalous Te inclusion size and distribution in CdZnTeSe, IEEE Trans. Nucl. Sci. 66 (11) (2019) 2329–2332.
[12] U.N. Roy, G.S. Camarda, Y. Cui, R. Gul, A. Hossain, G. Yang, J. Zazvorka, V. Dedic, J. Franc, R.B. James, Role of selenium addition to CdZnTe matrix for room-temperature radiation detector applications, Sci. Rep. 9 (1) (2019) 1620.
[13] O. Zelaya-Angel, J.G. Mendoza-Alvarez, M. Becerril, H. Navarro-Contreras, L. Tirado-Mejıa, On the bowing parameter in $Cd_{1-x}Zn_xTe$, J. Appl. Phys. 95 (11) (2004) 6284–6288.
[14] S.K. Chaudhuri, M. Sajjad, J.W. Kleppingar, K.C. Mandal, Correlation of space charge limited current and γ-ray response of $Cd_xZn_{1-x}Te_{1-y}Se_y$ room-temperature radiation detectors, IEEE Electron. Device Lett. 41 (9) (2020) 1336–1339.
[15] S.K. Chaudhuri, M. Sajjad, J.W. Kleppingar, K.C. Mandal, Charge transport properties in CdZnTeSe semiconductor room-temperature γ-ray detectors, J. Appl. Phys. 127 (24) (2020), 245706.
[16] U.N. Roy, G.S. Camarda, Y. Cui, R. Gul, A. Hossain, G. Yang, J. Zazvorka, V. Dedic, J. Franc, R.B. James, Evaluation of CdZnTeSe as a high-quality gamma-ray spectroscopic material with better compositional homogeneity and reduced defects, Sci. Rep. 9 (1) (2019) 7303.
[17] U.N. Roy, G.S. Camarda, Y. Cui, R.B. James, Performance study of virtual frisch grid CdZnTeSe detectors, Instruments 6 (4) (2022) 69.
[18] J. Byun, J. Seo, B. Park, Growth and characterization of detector-grade CdMnTeSe, Nucl. Eng. Technol. 54 (11) (2022) 4215–4219.
[19] B. Park, Y. Kim, J. Seo, K. Kim, Effectiveness of parylene coating on CdZnTe surface after optimal passivation, Nucl. Eng. Technol. 54 (12) (2022) 4693–4697.
[20] L. Brualla, M. Rodriguez, J. Sempau, Energy Spectra of Varian Linacs, 2012. https://www.primoproject.net/primo/.
[21] J.H. Hubbell, S.M. Seltzer, X-Ray Mass Attenuation Coefficients, 2004. https://www.nist.gov/pml/x-ray-mass-attenuation-coefficients.
[22] C.K. Mandal, S.H. Kang, M. Choi, A. Kargar, M.J. Harrison, D.S. McGregor, A.E. Bolotnikov, G.A. Carini, G.C. Camarda, R.B. James, Characterization of low-defect $Cd_{0.9}Zn_{0.1}Te$ and CdTe crystals for high-performance frisch collar detectors, IEEE Trans. Nucl. Sci. 54 (4) (2007) 802–806.
[23] S.U. Egarievwe, K.-T. Chen, A. Burger, R.B. James, C.M. Lisse, Detection and electrical properties of Cd 1−xZn xTe detectors at elevated temperatures, J. X Ray Sci. Technol. 6 (4) (1996) 309–315.
[24] S. Yang, M. Han, Y. Shin, J. Jung, Y. Choi, H. Cho, S. Park, Study on the applicability of semiconductor compounds for dose measurement in electron beam treatment, J. Korean Radiol. Soc. 14 (1) (2020) 1–6.
[25] L.A.R. da Rosa, D.F. Regulla, Ute A. Fill, Reproducibility study of TLD-100 microcubes at radiotherapy dose level, Appl. Radiat. Isot. 50 (3) (1999) 573–577.
[26] Y.J. Heo, K.T. Kim, M.J. Han, C.W. Moon, J.E. Kim, J.K. Park, S.K. Park, Development of a stable and sensitive semiconductor detector by using a mixture of lead (II) iodide and lead monoxide for NDT radiation dose detection, J. Instrum. 13 (3) (2018), C03023.
[27] B. Park, Y. Kim, J. Seo, J. Byun, K. Kim, Passivation effect on large volume CdZnTe crystals, Nucl. Eng. Technol. 54 (12) (2022) 4620–4624.